Development of an Intelligent Robot-Assisted System for Femur Fracture Alignment Using a Stewart Platform

by

Almira Askhatova

Submitted to the Department of Robotics and Mechatronics
in partial fulfillment of the requirements for the degree of

Master of Science in Robotics

at the

NAZARBAYEV UNIVERSITY

Apr 2025

Author .....
Department of Robotics and Mechatronics
Apr 29, 2025

Certified by .....
Ton Duc Do
Associate Professor
Thesis Supervisor

Accepted by .....
Yelyzaveta Arkhangelsky
Dean, School of Engineering and Digital Sciences

Development of an Intelligent Robot-Assisted System for Femur Fracture Alignment Using a Stewart Platform

by

Almira Askhatova

Submitted to the Department of Robotics and Mechatronics
on Apr 29, 2025, in partial fulfillment of the
requirements for the degree of
Master of Science in Robotics

Abstract

Being one of the most complex orthopedic injuries, femur fractures are the ones associated with prolonged recovery, high pain rates, and a strong requirement for precise alignment and optimal healing. Current methods for reduction rely heavily on manual manipulation and real-time fluoroscopy, often resulting in suboptimal alignment, increased radiation exposure, and prolonged procedural time. Despite technological advances in surgical robotics, few systems have addressed these shortcomings in a way that combines precision, automation, and safety. In response to these limitations, this thesis presents an autonomous robotic system for femur fracture reduction that integrates machine learning for actuator noise compensation.

This research proposes a novel robot-assisted intelligent system for fracture reduction based on a Stewart platform architecture, integrating real-time sensor feedback and data-driven pose correction. A 3D model of the fractured femur is reconstructed using 3D Slicer, and MATLAB algorithms analyze the bone geometry to identify key anatomical features, such as peaks and troughs. Due to the inherent inaccuracy of physics-based solutions derived from incremental encoder data and non-linear mechanical deflection not accounted for by inverse kinematics, a machine learning model is introduced to estimate and correct pose errors based on empirical IMU feedback. A machine learning model is trained using this data to predict optimal Stewart platform leg adjustments based on the required alignment.

Preliminary results suggest that machine learning-enhanced FK improves pose tracking accuracy over traditional methods, creating a more robust and adaptive control framework for robotic orthopedic interventions. This research contributes to the advancement of autonomous tele-surgeries, offering a data-driven approach to complex bone alignment procedures with the potential for minimal to zero surgeon assistance.

Thesis Supervisor: Ton Duc Do
Title: Associate Professor

Contents

List of Figures

Chapter 1

Introduction

Femur fractures are among the most serious and common orthopedic injuries, often resulting in significant pain, disability, and long recovery periods. As the longest bone in the human body, the femur, also referred to as the long bone or thigh bone, consists of three main regions, each with its attachments and landmarks: the proximal (upper end), femoral shaft (diaphysis), and distal part (lower end) as demonstrated of Figure 1-1 [1].

Categorized by the location along these of the femur bone, femur fractures usually include the proximal femur fracture, the femoral shaft fracture, and the supracondylar femur shaft fracture. The fracture of the proximal femur is often referred to as the hip fracture often occurs in the elderly population, particularly in the femoral neck—a vulnerable region due to its role in bearing significant mechanical stress. The neck of femur fractures (NORs) are the fractures in the proximal bone fragment and tend to be sustained by the elderly population. The femoral neck is one of the most vulnerable regions to fractures because it bears significant mechanical stress while supporting the weight of the human body, particularly during standing, walking, and high-impact activities. Its relatively thin structure and reduced vascular supply further contribute to its susceptibility to fractures, especially in elderly individuals with osteoporosis [7]. In addition to the increasing trends in the incidence of NORs, they are the ones associated with life-threatening complications such as pneumonia or deep venous thrombosis [8, 9, 10]. Since the larger portion of the proximal femur

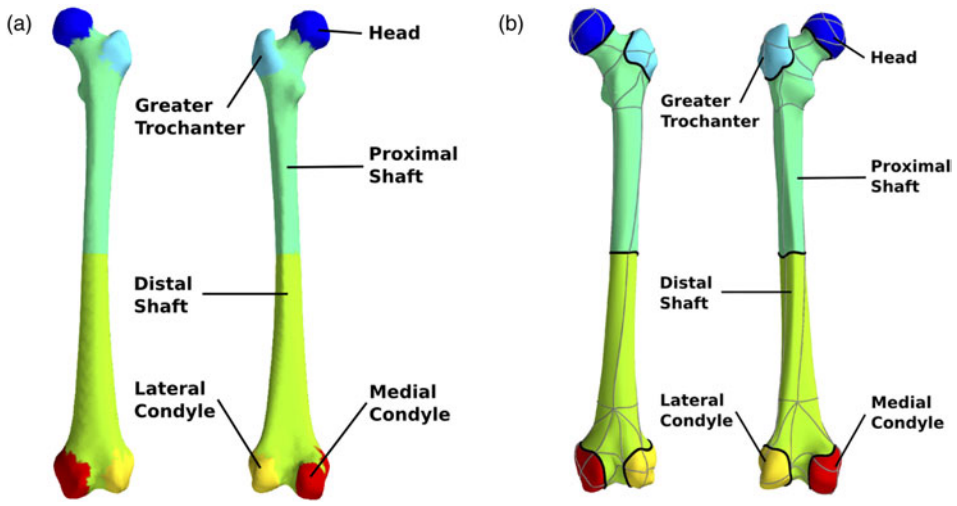

Figure 1-1: The regions of the femur bone [1]

fractures accounts for the elderly population aged over 70 years, current trends of prolonged life expectancy lead to an inevitable increase in this fracture incidence in the future and nearly doubling by 2050 [11, 12]. Moreover, the current trends indicate an increased level of frailty among femur fracture patients [13]. Frailty refers to the dynamic biopsychosocial syndrome in which there are reduced physiological reserves and impaired ability to regain homeostasis after a stressor event.

Additionally, femur fractures can be categorized by the type of injury and the patterns of the fracture and include the following:

1. Transverse Fracture – a clean break occurred across the shaft, aligning in a straight line within the femoral shaft.

2. Oblique Fracture – a diagonal break (angled line) across the bone.

3. Spiral Fracture – a twisting injury encircling the femoral shaft causing a corkscrew-like break.

4. Comminuted Fracture –the bone breaks into multiple fragments as the result of high energy impact.

5. Segmental Fracture – two distinct fractures within the same shaft.

The visual representation of these fracture types is illustrated in Figure 1-2.

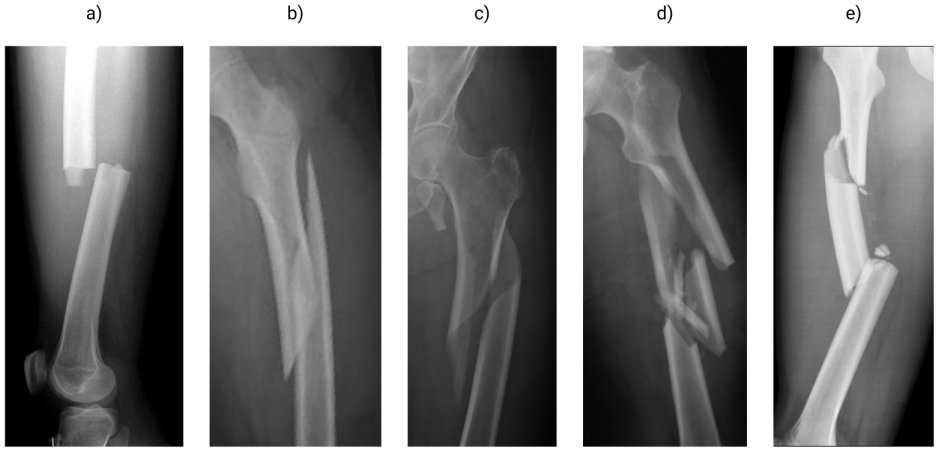

Figure 1-2: The classification of the femur fractures by the injury type: a) transverse fracture [2], b) oblique fracture [3], c) spiral fracture [4], d) comminuted fracture [5], e) segmented fracture [6]

Additionally, fractures are differentiated by closed (when the skin around the fracture is intact) and open (when a broken fragment of the bone punctures the skin). Due to the femur's critical role in weight-bearing and mobility, surgical intervention is often unavoidable to ensure proper alignment, stability, and functional recovery.

1.1 Background and Motivation

1.1.1 Incidence of femur fractions

Globally, the incidences of hip fracture range between 100 (as seen in South Africa) and 500 (in Denmark) per 100,000 people [7]. The one-year mortality rate after a hip fracture averages around 22 percent worldwide, with a range of 18 to 27 percent depending on the country. Mortality rates are influenced by factors such as age, access to medical care, and post-fracture complications. Loss of functional independence following a hip fracture is a significant concern, with approximately 30 to 50 percent of patients unable to regain their previous level of independence [7]. Many require

long-term care, rehabilitation, or assistance with daily activities. Patients who suffer a hip fracture are also at an increased risk of subsequent fractures. Approximately 8 percent experience another fracture within one year, 15 percent within two years, and 25 percent within five years [14]. Despite the risk of further fractures, post-fracture treatment rates remain low. Only 16 to 21 percent of patients receive pharmacological treatment, such as osteoporosis medications, after their fracture [15]. Although these medications can reduce the risk of another fracture by 30 to 50 percent, they remain underprescribed, with adherence to treatment declining in both the United States and Europe. Geographical trends in femur fractures indicate that urbanization is linked to higher fracture rates. In the Asia-Pacific region, hip fractures are increasing due to aging populations, while in Europe and North America, some decline in incidence has been observed, although rates remain high [16]. The risk of femur fractures increases significantly with age. People aged 65 and above are at the highest risk, with the 85-plus age group experiencing the highest mortality rates following a fracture. Given the current trends of aging of the overall population, the incidence of the femur fracture will only increase in the future. These statistics highlight the global burden of femur fractures and the need for improved surgical outcomes and post-fracture care.

1.1.2 Limitations of current manual methods and robotic-assisted systems

Patients with fractures should receive prompt treatment to prevent complications such as nonunion, avascular necrosis, or premature mortality [17]. Typically, to restore the proper functioning of the broken thigh bone and align the displaced fragments, surgery is performed. Femur fracture surgeries vary in their level of invasiveness, ranging from minimally invasive techniques (closed surgery) to fully open procedures (open surgery). While differing in the presence and extent of an incision, both surgical approaches share the same goal of achieving bone union in the most anatomically natural position. There are globally recognized principles and practices for treating femoral fractures diverging depending on the specific type of fracture and anatomical

specificity of the patient. The American Academy of Orthopaedic Surgeons (AAOS) has established evidence-based clinical practice guidelines for various types of femur fractures [18]. Prior to any femur alignment surgery, patient undergoes a physical exam followed by the X-Ray of the fracture to classify the fracture and mitigate the risk of further injury. Next, based on the state of fracture and surrounding tissue damage and other aspects, a personalized treatment plan is formed to achieve a high rate of alignment and fewest complications.

The complications of femur bone fractures are further enhanced by the challenges possessed by manual bone repositioning. Limited by tactile feedback and poor regulation of force application, the manual reduction increases the risk of bone misalignment and malrotation [19], potentially leading to improper load distribution, joint dysfunction, and the need for corrective surgeries. The challenges are particularly pronounced in the presence of ascertained anatomical abnormalities and complex fracture patterns. Moreover, the muscle contractures and soft tissue swelling that naturally follow the fracture, make it more difficult for the surgeons to reposition the fractured fragments [19].

With regard to the robot-assisted methods for fracture alignment, the robotic systems struggle from key challenges related to biomechanical variability, system limitations, and the complexity of real-world surgical environments. One of the primary issues is the difficulty in accounting for patient-specific anatomical variations, such as specificities in bone structures, soft tissue interactions, and fracture patterns. Unlike rigid industrial applications, where robotic systems operate in controlled conditions, orthopedic surgery involves dynamic biological tissues that can shift unpredictably due to muscle tension, swelling, or involuntary patient movement. These factors introduce variability that is difficult to compensate for using pre-programmed robotic trajectories.

Another major limitation is the reliance on static preoperative imaging, such as CT scans, for planning the alignment procedure. While preoperative images provide high-resolution 3D models of the fractured bone, they do not capture intraoperative changes in the fracture's position caused by patient movement, soft tissue deforma-

tion, or surgical manipulation. This results in a mismatch between the planned alignment and the actual intraoperative condition, leading to errors in robotic execution. Since most current robotic-assisted systems lack real-time adaptation mechanisms, they struggle to dynamically adjust for these discrepancies.

The precision of robot-assisted alignment is also affected by system noise, mechanical inaccuracies, and external forces. Actuators in robotic platforms experience errors due to backlash, friction, and thermal expansion, which can cause slight deviations in movement. Additionally, the effects of gravity and uneven load distribution on the fractured femur introduce misalignment forces that are difficult to model in real-time. Many current systems do not incorporate effective feedback loops to compensate for these disturbances, making it challenging to maintain accurate positioning throughout the procedure.

Furthermore, current robotic systems often lack effective real-time force sensing and adaptive control strategies. Proper fracture reduction requires careful force application to bring the bone segments into alignment without causing excessive stress on surrounding soft tissues. Existing robotic systems typically follow predefined motion trajectories based on kinematic calculations rather than continuously adjusting their movements based on force feedback. Without a real-time adaptive control mechanism, these systems may fail to achieve a perfect fit, particularly in complex or comminuted fractures where precise positioning is crucial.

1.2 Problem Statement

Achieving precise anatomical alignment in complex fractures remains challenging due to the intraoperative variability. Manual realignment methods are time-consuming and dependent on repeated fluoroscopic imaging, increasing radiation exposure. Current robotic-assisted systems lack adaptability for long-bone alignment, requiring real-time intelligent control.

Traditional control methods rely on forward and inverse kinematics, which assume ideal mechanical conditions and accurate actuator feedback. However, incremental

encoders introduce cumulative drift, and real-world factors such as structural deformation, backlash, and noise reduce positioning accuracy.

To improve real-time pose estimation of the Stewart platform, we propose a data-driven approach where an MPU sensor is mounted on the moving platform to capture inertial data (acceleration and angular velocity), while encoder-based actuator lengths are recorded simultaneously. Using this dataset, we aim to train a machine learning model that predicts the correction offset (pose error) to improve the platform's forward kinematics estimate.

This correction model will be applied on top of the classical kinematics-based pose estimation to achieve more accurate, robust platform control, especially in applications where mechanical inaccuracies cannot be fully compensated analytically.

1.3 Research Objectives

This research primarily focuses on three main objectives: 1) propose a robotic system for efficient and precise femur bone fracture alignment, 2) employ machine learning to account for the sensor noise and make the device adaptive to real-time adjustments, 3) develop a path planning algorithm that ensures smooth and safe reduction.

The first objective establishes the hardware and mechanical framework required for the robotic system, ensuring stable positioning and reduced alignment errors, the second objective forms the foundation for further optimization. The second objective fills the gap between rigid design dynamical nature of real-world surgical scenarios by implementing artificial intelligence. Not only is this anticipated to mitigate possible sensor noise but also enhances the self-reliance of the robot. Lastly, the third objective is responsible for providing an efficient and collision-free path, ensuring safe operation and eliminating the possibility of harming the soft tissues. The objective of this research is to enhance the pose estimation accuracy of a Stewart platform by integrating classical forward kinematics with a machine learning-based correction model. The study aims to collect synchronized data from incremental encoders and an MPU6050 inertial sensor mounted on the moving platform to establish a relation-

ship between actuator lengths and the actual orientation and position of the platform. This data will be used to train a regression-based machine learning model capable of predicting pose errors caused by mechanical imperfections such as backlash, joint flexibility, and encoder drift. The final objective is to validate the effectiveness of the correction model in improving pose estimation compared to traditional forward kinematics alone, enabling more precise control of the platform in critical applications such as surgical alignment.

1.4 Thesis Layout

The thesis work is further structured in the following way:

- Chapter 2: Literature Review explores existing research on robotic-assisted orthopedic surgery, Stewart platforms, machine learning applications, and path planning algorithms.
- Chapter 3: System Design and Methodology details the design of the robotic system, including hardware and software components, ML model development, and path planning strategies.
- Chapter 4: Experimental Setup describes the data collection process, training procedures, and testing methodologies for evaluating system performance. This chapter further summarizes the future directions for development.

Chapter 2

Literature Review

The integration of robotics into orthopedic surgery started mid 1980's and from that time revolutionized the way bone fractures are diagnosed, planned, and treated. Robotics enhances precision, improves repeatability, and reduces intraoperative complications [20, 21, 22]. While much of the focus has been on joint replacement and spinal procedures, the use of robotic systems for bone fracture (RAFR) alignment remains an emerging field, with only few research articles with a specific focus on robot-assisted orthopedics.

2.1 Robotics in Orthopedic Surgery

Orthopedic surgery has increasingly adopted robotic assistance for procedures requiring high precision. Early robot-assisted orthopedic surgeries (RAOS), such as ROBODOC [23], were primarily developed for total hip arthroplasty, enabling accurate bone resection and implant placement. Over the years, robotic applications expanded to knee arthroplasty, spinal surgery, and trauma management. Systems like MAKO and ROSA have become widely used for joint replacement, incorporating preoperative imaging and intraoperative navigation for improved surgical accuracy [24, 25, 26].

2.2 Bone fracture alignment robots

As the most common type of trauma, bone fractures creates a substantial operational burden on healthcare systems [27]. Despite significant advancements in orthopedic robotics, fracture alignment remains a challenging task with many important parameters requiring thorough consideration and accurate modeling [24]. For instance, in robot-assisted joint replacement surgeries, like total knee arthroplasty, predefined bone cuts are made, resulting in more reproducible component positioning and reduced alignment outliers compared to manual techniques [28]. Bone fractures, on the other hand, are highly variable (especially those that are results of high-energy trauma), requiring adaptability and real-time adjustments. Robotic systems for bone fracture reduction must account for multiple factors, including bone fragment displacement, rotational misalignment, and soft tissue constraints and thorough modeling for each of the tissue in the bone region (ligaments, muscles, tendons, articular cartilage). While some robotic solutions have been introduced for fracture alignment, they remain underutilized compared to joint replacement systems [29].

Bone fracture reduction involves aligning broken bone fragments before fixation. Traditionally, orthopedic surgeons perform closed reduction, where manual manipulation is used to realign the bone, or open reduction, which requires surgical exposure and fixation with plates, screws, or rods. Manual procedures rely heavily on the surgeon's expertise and often result in alignment errors such as rotational deformities, length discrepancies, and excessive soft tissue damage. Robotic-assisted fracture alignment systems aim to improve precision and reduce complications by incorporating real-time imaging, force feedback, and autonomous control mechanisms.

Several robotic systems have been developed for fracture alignment, each integrating different levels of automation and surgeon invasiveness levels. For instance, [30] introduced a 6 DOF robotic device for thigh bone fracture alignment. The navigation method relies on Cartesian coordinate-based control, ensuring smooth, precise movements for the fracture reduction process. The trajectory navigation is achieved using six independent linear actuators to manipulate the femur segment, allowing

controlled movements in all degrees of freedom. However, limitations include complex setup requirements, potential mechanical instability, and challenges in real-time adjustment during surgery [30]. On the other hand, [31] decided to focus on parallel mechanism based actuation instead of serial or hybrid approaches.The study developed an explicit inverse kinematic solution to guide a five-step reduction-fixation procedure, optimizing bone fragment positioning while minimizing soft tissue damage and radiation exposure. Unlike previous approaches, this system integrates high stiffness, precision, and six degrees of freedom (DOF), ensuring controlled fracture realignment. One key innovation is that after fracture reduction, the robotic structure can be locked to function as an external fixator, reducing the need for additional stabilization devices. However, its limited adaptability to complex fracture patterns and restricted workspace pose challenges, requiring further refinements for broader clinical application.

2.3 Advantages of Robotic-Assisted Fracture Reduction

Robotic systems in fracture alignment offer several advantages over conventional methods. Precision is significantly improved through preoperative imaging and real-time fluoroscopic feedback, which ensures accurate alignment and minimizes post-operative complications. While considered a gold standard and the most preferable method, closed reduction remains technically challenging to perform [32]. Closed fracture reduction requires continuous force application by the surgeon, leading to fatigue and potential inconsistencies. Robotic systems alleviate this burden by autonomously applying controlled forces, allowing for more consistent alignment across multiple cases.

Robotic systems optimize imaging protocols, reducing unnecessary exposure for both the patient and the surgical team. The repeatability of robotic movements ensures that fracture reductions follow algorithmically optimized procedures, elimi-

nating errors caused by manual inconsistencies. Additionally, robotic systems apply minimal force to bone fragments, preserving surrounding soft tissues, nerves, and blood vessels, which is particularly important in complex fracture cases.

2.4 Challenges and Limitations of Current Robotic Systems

Despite innovative strategies in control and trajectory generation, the primary challenges in utilizing RAFR stem from the complexity and invisibility of fractured bones, making precise alignment difficult [33]. Achieving a high level of precision in fracture reduction is crucial for ensuring optimal postoperative function. Additionally, the robotic system must provide an adequate workspace with an appropriate degree of freedom (DOF) to maneuver effectively. Sufficient output force is also necessary to handle the reduction process, particularly for lower extremity fractures [33].

Furthermore, the high cost of robotic platforms and the need for specialized training limit their widespread adoption, particularly in resource-limited settings. Many existing robotic systems operate in semi-autonomous mode, requiring continuous supervision by a surgeon. Fully autonomous systems capable of managing complex fractures without human intervention remain a technological challenge.

The variability of fracture patterns presents another further challenges the field of RAFR [33]. Unlike joint replacement procedures, where bone cuts follow predefined surgical plans, fracture alignments require adaptability to different displacement patterns and bone fragment configurations. Current robotic systems struggle with real-time decision-making in highly variable cases, necessitating further advancements in AI-driven adaptive planning. Another significant challenge is the integration of robotic systems into existing surgical workflows. Many orthopedic surgeons are reluctant to adopt robotic technology due to unfamiliarity with robotic interfaces, increased intraoperative setup time, and potential disruptions to conventional surgical techniques.

2.4.1 Pose Estimation Accuracy Challenges

Accurately determining the 3D pose of fractured femur segments remains a huge problem. Current systems usually rely on rigid fixation pins with optical trackers or preoperative imaging to gauge bone position, but these methods are prone to error. For example, heavy reduction forces (often exceeding 400 N) can bend the orthopedic pins, introducing tracking errors that lead to misalignment during reduction [34]. Even when using advanced vision-based tracking, residual errors are on the order of millimeters. One prototype using binocular cameras achieved about 2 mm translational error and 3° angular error in alignment [35], while a parallel manipulator on a traction table reported best-case positioning errors of about 0.63 mm under fine adjustment [35]. Such accuracy, achieved in controlled settings, may deteriorate in real surgical conditions with obstructions or soft tissue interference. In practice, optical navigation systems still show average position errors of around 1–2 mm [35], which, although clinically acceptable, indicates a gap between ideal alignment and what current systems can reliably measure. In short, reliably obtaining sub-millimeter, high-confidence pose estimates of bone fragments in real time remains an unsolved challenge.

2.4.2 Forward/Inverse Kinematics Limitations

Stewart platform (hexapod) mechanisms introduce unique kinematic difficulties that existing literature addresses only partially. Inverse kinematics (computing required actuator lengths for a desired pose) is straightforward, but the forward kinematics (deriving the platform pose from given actuator lengths) is notoriously complex. Solutions typically require iterative numerical methods that depend on a good initial guess [35]. An inappropriate initial pose can slow down convergence or even lead to incorrect pose solutions. This sensitivity means that real-time pose verification is non-trivial, and the robot may struggle to know its exact configuration without lengthy computation. Moreover, Stewart platforms have multiple solutions and can encounter singular configurations where the mechanism loses degrees of freedom. If

the platform approaches a singular pose, the forward solver may fail to find a valid solution. , or small actuator motions can cause unpredictable jumps in platform orientation. These robots also suffer from a limited workspace relative to surgical needs. A traditional Stewart hexapod can only achieve a certain range of translation/rotation, which may not cover all possible fracture displacements. Researchers have noted that the parallel structure's operating space is inherently constrained – such hexapod devices are "only suitable for lower limb fracture reduction" and cannot accommodate more complex or proximal fractures due to workspace limits. Recent designs (e.g. tripod or hybrid mechanisms) have tried to expand the range of motion, significantly improving workspace compared to a classical Stewart platform [35]. However, even these acknowledge that further work is needed to make them clinically practical. In summary, solving the Stewart platform's forward kinematics robustly and handling its workspace/singularity limits are recognized gaps, making it difficult to fully automate bone alignment without manual intervention or very careful pre-planning.

2.4.3 Actuator Precision and Mechanical Constraints

Another technical gap lies in actuator precision and power limitations of Stewart platform reducers. Femur reduction demands both fine positional accuracy and the ability to exert high forces to overcome muscle tension. While hexapod-based external fixators have demonstrated sub-millimeter positioning accuracy in laboratory tests (median $<$0.3 mm error, 0.2° angular error) [36], achieving this precision on a patient requires extremely high-quality actuators and calibration. Many prototypes use DC motor-driven linear actuators, which introduce their own issues. Limited motor torque can cap the force the robot applies, and indeed some early hexapod systems had insufficient load capacity to reliably overcome muscle and tissue resistance [37]. One report notes that a motorized hexapod fixator, while highly precise, was "only suitable for long bone fractures" because motor power constraints led to poor force output [**?**]. To increase force, larger motors are needed, but they in turn create a bulky device that can jam or impede surgical access.

This trade-off between actuator power and size remains a bottleneck – current

Stewart platforms must either be heavy and unwieldy or struggle to apply adequate force. Precision control of each leg is also affected by mechanical play and calibration errors. Any backlash or flex in the actuator joints can introduce positioning error that accumulates at the bone. Researchers have begun modeling these mechanism errors: for instance, drive rod length errors and joint offsets can be converted into end-effector pose errors [38].

Without compensation, even small manufacturing tolerances will degrade reduction accuracy. Although calibration routines exist, they are often time-consuming and not performed in real time. Overall, ensuring each actuator moves exactly as commanded (with resolution on the order of 0.1 mm or better) under load is still challenging. Some groups have explored non-conventional actuators to address this – for example, an intrinsically compliant parallel manipulator using pneumatic muscles achieved high alignment accuracy while being less rigid [**?**]. Such approaches suggest that improving actuator technology (for both precision and force output) is key. The literature still lacks a consensus solution for compact, high-force, and high-precision actuation in these fracture reduction robots, marking it as a clear gap.

2.4.4 Control and Stability Challenges

Maintaining stable and safe control of a Stewart-platform reducer during surgery is difficult, and current systems only partially address this. One issue is controlling the reduction trajectory under unpredictable loads. The fractured femur may suddenly slip into alignment or resist movement due to soft tissue, and a purely position-controlled robot could overshoot or oscillate. This raises concerns about control stability and safety. Indeed, achieving "high-precision reduction" in the lab is one thing, but ensuring safety in vivo (avoiding soft-tissue damage or secondary fractures) is still an open problem [35]. Sudden jerks or excessive forces can injure the patient. Researchers have observed that surgeons operating robotic reducers lack haptic feedback of bone resistance, which can lead to unintentional injury. Unlike manual reduction, the robot does not inherently feel when it's pushing too hard. Although some systems incorporate six-axis force/torque sensors to monitor forces on

the bone, determining safe force thresholds in real time is non-trivial [36]. There is no clear consensus on the force limits that guarantee safety, so tuning a controller to be both effective and gentle is challenging. Stability is further tested by the need to react in real time to alignment errors. If the fracture starts to deviate or a pin loosens, the controller should ideally correct without causing oscillation. Classical PID control may not suffice if the system dynamics change (e.g., as muscle relaxes or as reduction progresses). Researchers have started implementing advanced control schemes to address this gap. For example, a 6-DOF force-feedback control with adjustable admittance was demonstrated to automatically limit forces to protect the bone [35]. This kind of impedance or admittance control helps the robot "back off" when resistance is high, mimicking a surgeon's delicate touch. However, such solutions add complexity and have mainly been tested in experimental settings. The literature suggests that many prototypes still operate in simplified conditions without fully robust, closed-loop force and motion control. Ensuring control stability – i.e. the robot moves smoothly to the target without overshoot, and can hold the reduction against muscle forces without vibrating or drifting – is a gap that needs more work. In summary, while basic controller implementations exist, the absence of proven, highly stable control strategies (especially those that account for patient-specific variability in real time) is a noted shortcoming of current Stewart platform fracture reduction systems.

2.4.5 Lack of Machine Learning and Adaptive Compensation

Another significant gap in current Stewart-platform-based reduction systems is the nearly complete absence of machine learning techniques for error correction or real-time adaptation. Existing systems rely on predefined kinematic models, calibrations, and simple feedback control without any form of learning-based improvement loop. For instance, if there are unmodeled errors (such as slight flex in the frame, or systematic offset in pose estimation), the robot does not "learn" from its mistakes across operations. Instead, any compensation is done via manual calibration or offline computations. Recent research has begun to recognize this issue: one study surveyed

intelligent optimization methods (genetic algorithms, neural networks, swarm intelligence, etc.) for robot accuracy improvement and noted that while such methods are theoretically available, they have not been applied to the pose error compensation of parallel robots in fracture reduction settings [38].

In other words, current femur reduction robots ignore machine-learning-based correction – there is no online model updating or AI-driven calibration happening during surgery. The pose estimation process in these systems is a clear example. Errors from imaging or tracking are handled by rudimentary means (e.g. assuming pins are rigid, or doing a one-time registration). If those assumptions break, the system doesn't adapt. A machine learning approach could, for example, use data from previous reductions to predict and correct systematic pose drifts or to fuse multiple sensors for a more accurate estimate. Yet, contemporary designs do not include such components. Some groundwork has been laid in related fields – for example, researchers have shown that stereo vision tracking enhanced by machine learning can locate markers with sub-millimeter accuracy [35] and neural-network-based error compensation has improved accuracy in industrial robotic arms [38].

However, these innovations are not integrated into present orthopedic robots. The literature so far describes no real-time learning-based correction loop for Stewart platform reducers. Compensation strategies, when present, use classical algorithms (e.g. optimized iterative methods) rather than adaptive machine learning models [38].

The consequence is that current systems cannot easily compensate for unexpected discrepancies – for instance, if the actual bone position deviates from the model due to pin slip or patient movement, the robot has limited means to adjust on the fly. This lack of an adaptive, intelligent control layer is a pronounced gap. In summary, Stewart platform fracture reduction robots today remain largely deterministic and pre-programmed. They lack machine-learning-driven error correction and real-time compensation models, which could otherwise refine pose estimation and control accuracy continuously. Addressing this gap – by incorporating learning algorithms for calibration, pose correction, and dynamic control tuning – is an important opportunity for future improvements in robotic orthopedic alignment [38].

Chapter 3

System Design and Methodology

3.1 System Hardware Setup

The figure 3-1 demonstrates the setup of the robot designed for automated femur bone fracture reduction. The setup features the surgical table where the patient is positioned supine, with specialized leg holders securing the legs to maintain stability during the procedure. The system further uses circular rings and adjustable rod that are attached to the bone passing through the soft tissues. The pins are under pressure to keep the soft tissue movement minimized. This also ensures stable gripping of the femur bone allowing for gradual adjustments. The setup provides secure fixation to the both distal and proximal fragments of the fractured bone. The Stewart platform is chosen for its inherent stiffness, spatial controllability, and compact footprint in surgical environments. The system enables simultaneous actuation in all six degrees of freedom, which was shown in prior studies to reduce realignment force and improve procedural outcomes.

While the proximal segment is staying rigid and unmoved, the distal part of the fractured bone is being manipulated to achieve a precise alignment with respect to the upper fragment. The specific reason for that is that the proximal region of the femur is firmly anchored with the acetabulum and surrounded by the hip joints and muscles (cite). Ligaments in that area (iliofemoral, ischiofemoral, and pubofemoral) provide significant stability, making it less mobile serving as a good reference point

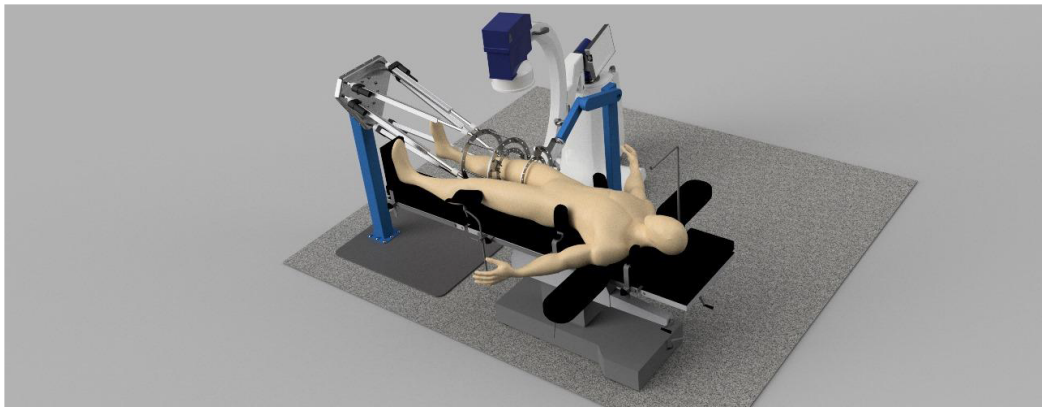

Figure 3-1: The setup of the robotic system

for fracture reduction.

The figure 3-2 displays the fixation of the distal segment of the fractured bone. The Ilizarov fixator consists of two concentric metal rings connected by threaded rods and adjustable bolts, which serve to stabilize and manipulate bone segments. In the center of the rings, a 3D-printed attachment piece is mounted to simulate the distal femur fragment. The structure is attached to multiple actuated rods, which are likely part of the Stewart platform, providing six degrees of freedom (DOF) for precise positioning. This allows for controlled adjustments in alignment based on machine learning predictions and sensor feedback.

The Ilizarov fixator is an external fixator commonly used in orthopedic surgery for bone lengthening, realignment, and fracture stabilization. It operates by using tensioned Kirschner wires (K-wires) or screws to secure bone fragments to external metal rings, which are connected via threaded rods. By adjusting the screws, the surgeon or robotic system can gradually apply controlled forces to move the bone fragments into proper alignment. This gradual correction method is particularly effective for complex fractures, bone deformities, and lengthening procedures. The design of the fixator in the image suggests that it is adapted for robotic manipulation, allowing for precise automated realignment of a fractured femur using controlled actuator movements. The combination of external fixation and robotic-assisted adjustments ensures high precision, minimizes surgical intervention time, and reduces the risks associated with manual realignment.

Figure 3-2: The attachment of the distal segment

Figure 3-3: The attachment of the proximal segment

The imaging device X-Ray, positioned centrally right above the patient, captures high-resolution, biplanar images that assist in ensuring the correct anatomical alignment of the femur. A control console or display screen to the right allows the surgeon to monitor the imaging data, observe the robotic arm's position, and make any necessary adjustments.

The Stewart platform is a parallel mechanism equipped with six actuators that provide six degrees of freedom, enabling controlled movements for precise femur alignment. It is mounted on a rigid base structure that ensures stability during operation. An IMU sensor is placed at the center of the platform's ring, capturing real-time motion data that aids in adjusting actuator lengths for proper alignment. The system also incorporates a C-arm imaging unit, providing real-time X-ray feedback to validate bone positioning. The overall setup is designed for precision, stability, and adaptability in orthopedic surgical environments.

3.2 System Operational Principle

The diagram on Figure 3-4 displays the operational workflow of the autonomous of the robot-assisted femur fracture reduction device. The main stages are designed as follows:

1. Pre-operative stage: during this stage the main surgery preparations are performed. The CT data is collected for 3D reconstruction and bone model processing and analysis. Furthermore, in this stage preparatory analysis for collecting necessary information for efficient and safe path planing is performed.

2. Motion planning stage: after the data is extracted, the IK algorithm is employed for the o determine the required actuator movements for bone alignment. In tandem with the machine learning model, which compensates for the uneven load distribution, sensor noise, and other uncertainties, they ensure smooth, tissue-aware motion for the robotic system.

3. Intra-operative stage: This stage consists of fixation of the bone segments with

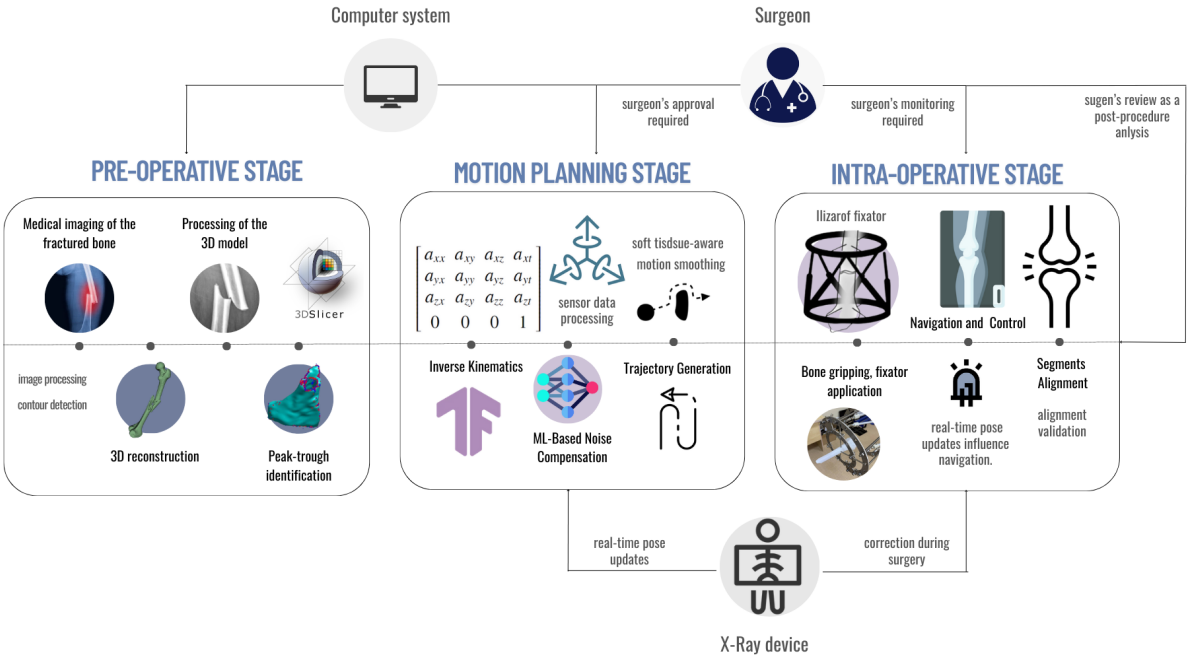

Figure 3-4: Operational flow of the robot-assisted femur fracture reduction device

the Ilizarof fixators for stabilization The system utilizes real-time navigation and control, continuously updating pose data based on intra-operative X-ray feedback. The final segments alignment is validated to confirm successful bone reduction.

3.3 Stewart Platform Kinematics

A parallel platform is composed of two main structural components: a stationary base plate and a movable upper platform, which are interconnected by six linear actuators. The relative positions of these components are uniquely determined by the spatial coordinates of these six connecting links, as illustrated in Figure 3-6. The vertices of the system are arranged to form an irregular polygon within a single plane.

Each link consists of a universal joint, which allows the platform to achieve complex motion. Its movement is controlled by adjusting the lengths of six actuators arranged in a hexapod configuration. In serial manipulators, solving the direct kine-

matics problem is relatively straightforward, while the inverse kinematics problem is more complex. However, for parallel manipulators, the situation is reversed. In the case of inverse kinematics, the given parameters include the position vector and the rotation matrix, and the objective is to determine the link lengths. Since the positions of the connection points, as well as the orientation and position of the moving platform, are already known, computing the link lengths becomes a more manageable task. Conversely, in the direct kinematics problem, the link lengths are provided, and the challenge lies in determining the position vector and rotation matrix of the moving platform.

For the Stewart Platform, solving the direct kinematics problem is particularly difficult because it involves a set of non-linear equations. The system typically has multiple real solutions, with at least eight possible outcomes. Direct kinematics refers to determining the position and orientation of the Stewart platform's end-effector (top platform) based on the given actuator lengths. This process requires solving a set of nonlinear equations, making it computationally complex. Direct kinematics is primarily used for validation and calibration purposes. In the final version of the system, the coordinates of the proximal bone segment will be known, and the objective will be to determine the corresponding actuator lengths, which necessitates the use of inverse kinematics.

3.3.1 Inverse Kinematics

Inverse kinematics, on the other hand, involves computing the required actuator lengths given a desired position and orientation of the end-effector. This is essential for controlling the Stewart platform in real-time, ensuring that the distal femur segment moves precisely as needed for alignment.

We define the rotation matrix $\mathbf{R}_z(\psi)$ where:

$$\begin{bmatrix} x' \\ y' \\ z' \end{bmatrix} = \mathbf{R}_z(\psi) \begin{bmatrix} x \\ y \\ z \end{bmatrix} \tag{3.1}$$

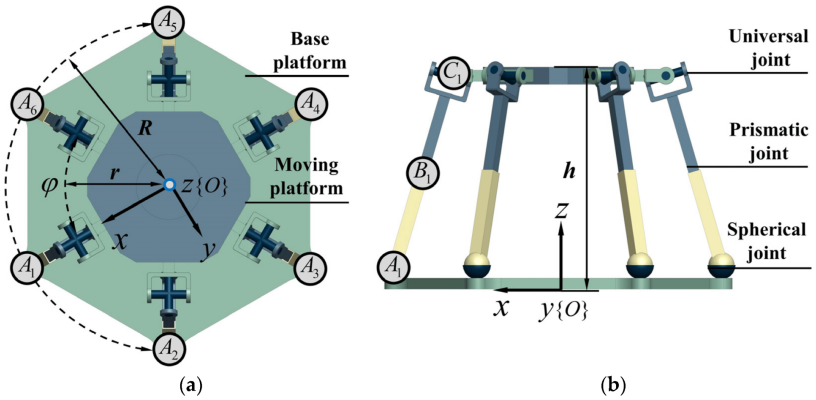

Figure 3-5: The overview of Stewart platform mechanism

and

$$\mathbf{R}_z(\psi) = \begin{bmatrix} \cos\psi & -\sin\psi & 0 \\ \sin\psi & \cos\psi & 0 \\ 0 & 0 & 1 \end{bmatrix} \tag{3.2}$$

This transformation alters the coordinates of the point while maintaining its position relative to the z-axis. Similarly, if we consider the second rotation θ represents the pitch transformation, which affects the x and z coordinates while keeping the y coordinate unchanged.

$$\mathbf{R}_y(\theta) = \begin{bmatrix} \cos\theta & 0 & \sin\theta \\ 0 & 1 & 0 \\ -\sin\theta & 0 & \cos\theta \end{bmatrix} \tag{3.3}$$

For rotations about the x-axis, the roll transformation is described by the matrix $\mathbf{R}_z(\psi)$, which modifies the y and z coordinates while the x coordinate remains constant.

$$\mathbf{R}_x(\varphi) = \begin{bmatrix} 1 & 0 & 0 \\ 0 & \cos\varphi & -\sin\varphi \\ 0 & \sin\varphi & \cos\varphi \end{bmatrix} \tag{3.4}$$

The overall rotation of the platform with respect to the base is determined by

the combined effect of these three rotations. The final transformation matrix $\mathbf{R}_(RB)$ is obtained by multiplying the individual rotation matrices in the order of rotation about the z-axis, followed by the y-axis, and finally the x-axis. The full rotation matrix of the platform relative to the base is given by:

$$\mathbf{P}_{RB} = \mathbf{R}_z(\psi)\mathbf{R}_y(\theta)\mathbf{R}_x(\varphi) \tag{3.5}$$

Expanding the multiplication:

$$\mathbf{P}_{RB} = \begin{bmatrix} \cos\psi & -\sin\psi & 0 \\ \sin\psi & \cos\psi & 0 \\ 0 & 0 & 1 \end{bmatrix} \begin{bmatrix} \cos\theta & 0 & \sin\theta \\ 0 & 1 & 0 \\ -\sin\theta & 0 & \cos\theta \end{bmatrix} \begin{bmatrix} 1 & 0 & 0 \\ 0 & \cos\varphi & -\sin\varphi \\ 0 & \sin\varphi & \cos\varphi \end{bmatrix} \tag{3.6}$$

Expanding this matrix multiplication step by step, we first apply the rotation about the z-axis, followed by the rotation about the y-axis, and finally the rotation about the x-axis. The result is a single composite rotation matrix that fully describes the orientation of the platform relative to the base. The next expression provides a detailed breakdown of how each coordinate is transformed through this sequential rotation process.

$$\mathbf{P}_{RB} = \begin{bmatrix} \cos\psi\cos\theta & -\sin\psi\cos\theta + \cos\psi\sin\theta\sin\varphi & \sin\psi\sin\varphi + \cos\psi\sin\theta\cos\varphi \\ \sin\psi\cos\theta & \cos\psi\cos\varphi + \sin\psi\sin\theta\sin\varphi & \cos\psi\sin\varphi + \sin\psi\sin\theta\cos\varphi \\ -\sin\theta & \cos\theta\sin\varphi & \cos\theta\cos\varphi \end{bmatrix} \tag{3.7}$$

The target position of the leg l_i is represented in Eq. 3.8, while the corresponding leg length is provided in Eq. 3.9.

$$\bar{l_i} = \overline{P_iB_i} = p + R_P^B \cdot b_i^P - a_i^B \tag{3.8}$$

$$|l_i| = \sqrt{(p + R_P^B \cdot b_i^P - a_i^B)^T \cdot (p + R_P^B \cdot b_i^P - a_i^B)} \tag{3.9}$$

Figure 3-6: The stewart platform as the part of the femur fracture reduction robot

In which, b_i^P represents the vector of joint point i between the leg i and the plate P; and the ith represents the vector of joint point i between the leg i and the plate B, for $i = 1, \ldots, 6$.

The lengths of six legs of the platform will determine the position and attitude of the top plate, so inversely, given any position and attitude of the top plate within its working space, the lengths of six legs can be calculated with Eq. 3.

3.4 3D Reconstruction of the Femur Fracture

As part of the preoperative stage, medical imaging techniques such as Computed Tomography (CT) are performed. The primary reason for choosing these medical imaging methods is that they provide detailed high-resolution information on the cross-sectional fragments which is crucial for the 3D reconstruction. Other techniques

like X-Ray are not capable of providing specific information suitable to assess the fracture in three dimensions, as the result not being able to create a solid computer-aided pre-operative planning and robot navigation. Magnetic Resonance Imaging (MRI), while highly effective for soft tissue visualization, is not typically used for bone fracture assessment due to several limitations. Unlike CT, which captures detailed bone structure with high spatial resolution, MRI primarily excels in imaging soft tissues such as cartilage, ligaments, tendons, and muscles. The signal from bones in MRI scans is often poor due to the low proton density in cortical bone, leading to insufficient contrast and a lack of clear fracture visualization. Additionally, MRI cannot provide the same level of sharp, high-resolution cross-sectional imaging of bone fragments, making it unsuitable for 3D reconstruction and precise geometric modeling of fractures. While MRI can be useful in detecting associated soft tissue damage, bone marrow edema, or occult fractures, it does not offer the necessary anatomical detail to accurately guide robotic navigation or surgical planning in bone realignment procedures. Therefore, CT remains the preferred imaging modality for preoperative assessment in cases requiring detailed bone reconstruction and robotic-assisted intervention.

The resulting files, typically stored in the DICOM (Digital Imaging and Communications in Medicine) format, contain cross-sectional slices of the body from three different planes, allowing for detailed visualization and analysis of the anatomical structures. File of this format can be 3D reconstructed using specialized software that applies segmentation techniques to efficiently isolate the region of interest - the hard tissues. The segmented data is arranged in a volumetric structure, where interpolation algorithms generate a continuous 3D representation from the discrete image slices. An example of reconstrcuted CT image of the pelvis and femur region is displayed on the Figure 3-7.

In this research the DICOM data is processed in 3D Slicer (refer to Figure) software to achieve a 3D structure following the procedure (8):

1. The medical data is uploaded to the software.

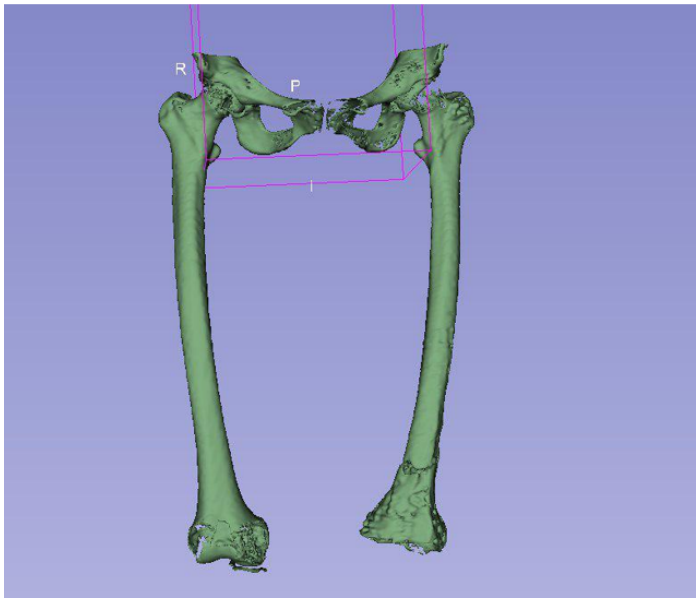

Figure 3-7: A 3D reconstructed pelvic and femur bones

2. The thresholding is applied with varying hyperparameters.

3. The excessive noise is cleaned out manually.

4. The resulting cleaned-out 3D hard tissue model is exported in stereolithography (STL) format.

This reconstructed model serves as a foundation for further computational steps aimed at achieving optimal alignment and stabilization. The limitation of this method for 3D reconstruction lies in the manual nature of 3D reconstruction through the software which becomes increasingly difficult with the noise in the image. This is especially usual for the images containing information on the bones with the presence of implants - the metallic part is highlighted in a brighter color making the other structures look much darker. This as well brings a lot of unessesary nois into the image bringing up the need for the manual removal of debris.

3.5 Feature Extraction

The 3D reconstructed models of the fractured femur serve as the input to the MATLAB-based algorithms for them to analyze the geometry of the femur to identify key

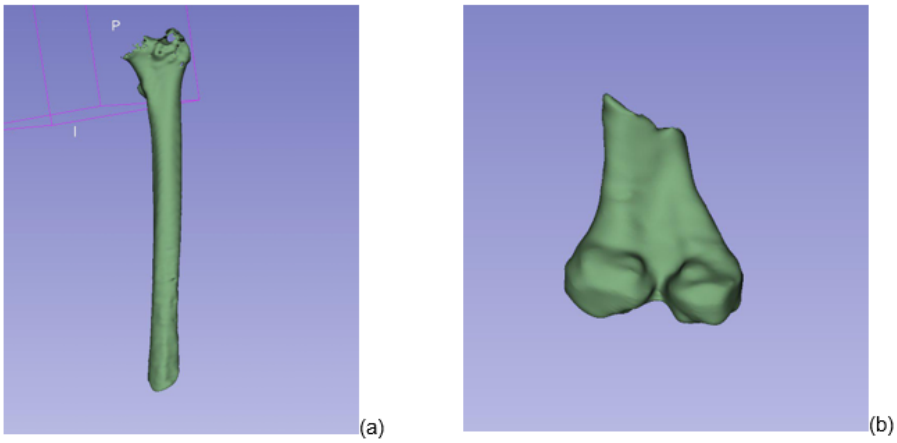

Figure 3-8: 3D reconstructed fractured femur models from CT scans. (a) Proximal fragment (b) Distal femur fragment.

anatomical features. The algorithm detects peaks, troughs, and fracture planes, helping to define the optimal alignment parameters. Feature extraction includes identifying the centroid of the bone fragment, computing fracture surface normal, and detecting critical misalignment points.

Feature extraction in this process involves analyzing the 3D geometry of the femur model to identify critical anatomical landmarks, specifically peaks and troughs, based on curvature analysis. The method begins by loading an STL model of the fractured femur and constructing a triangular mesh representation using the vertex and face connectivity data. To ensure computational efficiency, unused vertices are removed, and the cleaned mesh is visualized for inspection. The core of feature extraction relies on estimating the local curvature at each vertex by analyzing the variation in normal vectors of connected faces. The algorithm computes the deviation of each vertex's normal from the average normal of its neighboring faces, determining areas of high curvature change. Peaks, representing convex regions, are identified where the maximum curvature exceeds a defined threshold based on a statistical analysis of curvature values, while troughs, representing concave regions, are detected where the minimum curvature falls below a set threshold. These identified points are then plotted onto the 3D bone surface, providing insight into the geometric structure of the femur and serving as key reference points for further processing in fracture realignment

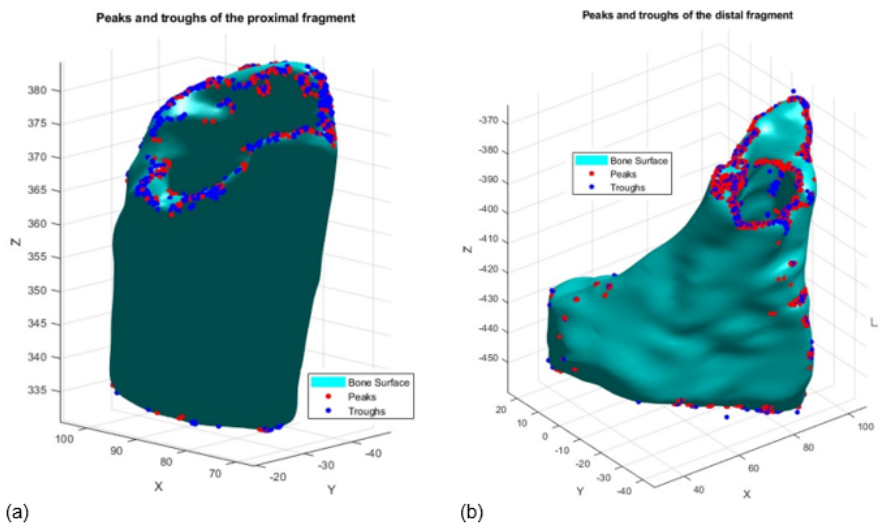

Figure 3-9: Curvature-based landmark extraction on bone fragments. (a) Peaks and troughs detected on the surface of the proximal femur segment. (b) Peaks and troughs detected on the surface of the distal femur segment.

and robotic-assisted surgical planning. Figure 3.5 presents the results of curvature analysis applied to both the proximal (a) and distal (b) femur fragments. The bone surface is visualized along with automatically detected surface landmarks, where red dots represent convex peaks and blue dots mark concave troughs. These geometrical features are critical for downstream alignment and registration tasks, serving as anatomical anchors during the reconstruction of the original femur geometry.

These extracted features serve as input for the machine learning model and path planning algorithm.

3.6 Methodology

Accurate pose estimation is critical for the Stewart platform in our femur fracture reduction robot, as even small pose errors can affect surgical outcomes. The Stewart platform's kinematics are highly nonlinear and coupled, which makes purely model-based pose calculation prone to errors if the mechanism is not perfectly calibrated. To address this, we develop a data-driven correction model. The following subsections

detail the methodology, including data collection from the robot, definition of ground truth pose, preparation of training data, the machine learning model design, training procedures, evaluation metrics, and how the learned model is integrated into the real-time operation.

3.7 Machine Learning Model for Stewart Platform Control

The primary goal of machine learning for the implementation of the femur fracture reduction robot is to ensure that the system compensates for unnessesary noise and other imperfections in the face of gravity and extra loads. Traditional inverse kinematics methods alone may struggle to account for small variations caused by mechanical tolerances, sensor noise, soft tissue deformation, and unpredictable external forces. Machine learning enhances the system's ability to predict the optimal final alignment by learning from a combination of simulated and real-world data, ensuring that each adjustment made by the Stewart platform remains within biomechanical constraints. By incorporating sensor feedback, such as IMU data and force measurements, the model dynamically refines actuator movements to maintain precision even in cases where traditional control methods might introduce small but significant errors. This capability is particularly crucial given that external forces, such as the weight of the leg and fixator adjustments, can introduce deviations that would otherwise require manual correction. Furthermore, machine learning allows for real-time adaptability, enabling the system to make micro-adjustments to optimize alignment without requiring excessive computational power for iterative kinematic recalculations. By integrating physics-informed constraints with data-driven learning, the model ensures that the robotic system remains robust, efficient, and capable of performing accurate femur realignment while minimizing stress on the patient and reducing overall procedure time.

To predict and correct pose estimation errors caused by real-world inaccuracies in

actuator feedback and mechanical imperfections by learning the relationship between actuator lengths and the true platform pose. Theoretically, the inverse kinematics module calculates the theoretical actuator lengths required to achieve the desired final position and orientation, while forward kinematics reevaluates the resulting pose using these computed actuator lengths. However, the problem is that these calculations assume an idealized, noise-free, rigid system, whereas in reality, several factors introduce deviations. System noise affects sensor readings, load variations influence actuator performance due to the weight of the femur and fixator constraints, and gravity compensation is necessary because the femur is not a rigid body in a vacuum, meaning external forces dynamically shift the alignment. Further inaccuracies are introduced by the effects of the encoder drifts, joint backlash, mechanical deformation and deflection of the Stewart platform legs, and calibration imperfections.

Machine learning is introduced to compensate for these unmodeled errors rather than to replace the kinematic equations. Instead of computing link lengths, the ML model learns the discrepancy between the predicted and actual positions based on real-world data. Given a known desired pose, the ML model predicts how much external factors, system noise, and modeling inaccuracies will distort the outcome. It then applies this correction to the final actuator lengths to ensure a more accurate alignment. The Motion Processing Unit (MPU) measures the real-world pose using IMU sensors, providing the actual position and orientation. Comparing the model's predicted pose to the real measured pose allows the ML model to continuously refine its predictions, improving accuracy over time.

This approach creates a hybrid system where kinematics provides the theoretical foundation, and ML refines the solution by learning real-world deviations. This aligns well with the use of a Physics-Informed Neural Network (PINN), where machine learning is guided by both physical equations and empirical corrections. The integration of ML ensures that the robotic femur alignment system accounts for uncertainties, improving precision beyond what traditional kinematics alone can achieve.

Machine learning is necessary to predict noise at different regions because the noise is not uniform across all positions of the Stewart platform ring. The primary reason

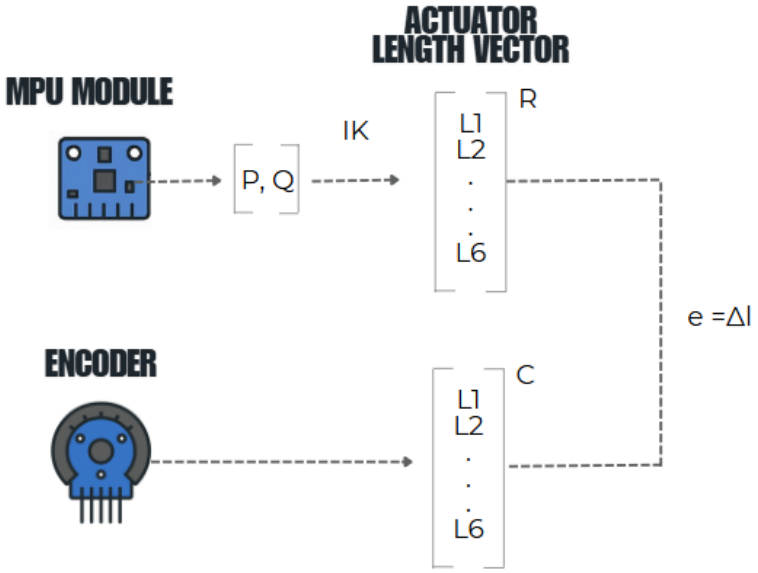

Figure 3-10: Error compensation architecture for stewart platform-based femur alignment

for this variation lies in the differences in orientation, load distribution, and gravity effects at each position. The Stewart platform operates with six degrees of freedom, including three translational and three rotational movements. When the ring moves to different orientations, the actuators experience varying mechanical stresses, which affect their accuracy. The angle of force application changes, leading to different actuator responses, while joint friction and backlash vary depending on the orientation, introducing inconsistent errors. Since the platform's mechanical imperfections and actuator dynamics are orientation-dependent, the noise pattern is different at each configuration.

The femur is not a uniform load, and its weight distribution changes based on the position of the fractured segment. As the Stewart platform moves, the lever arm effect shifts, altering how forces are applied to each actuator. Fixators and soft tissues introduce additional external forces that affect movement accuracy, meaning that force distribution is not constant, and system noise varies across different positions. Gravity further influences how actuators compensate for weight at different angles. When the ring is tilted, some actuators work harder than others, causing deviations.

Gravity-induced sagging creates nonlinear displacement errors, which cannot be captured using static equations. These errors are not explicitly modeled in traditional kinematic equations, making a data-driven machine learning approach necessary to learn the position-dependent noise patterns and apply corrections dynamically.

A purely physics-based error compensation model would require an extensive manual calibration process for every possible configuration of the Stewart platform. Since error patterns are complex and nonlinear, traditional mathematical modeling would be inefficient. Machine learning enables the system to learn the error distribution across different poses automatically, generalize to new configurations, and refine predictions over time based on new data. The noise affecting the Stewart platform is not constant for each position of the ring but varies due to orientation changes, load redistribution, and gravitational effects. Without machine learning, traditional kinematic calculations would result in systematic alignment errors that cannot be fully eliminated.

3.7.1 Data Collection

The figure 3-11 illustrates the whole system operation for the data collection. In this system, data collection is carried out through the coordinated operation of several embedded devices. The Arduino Mega is responsible for controlling six motors and monitoring their positional feedback using rotary encoders. It periodically serializes the encoder data into a JSON format and transmits it via UART to an ESP8266 module. The ESP8266 acts as a wireless bridge, receiving the encoder data, validating its structure using a lightweight JSON parser, and forwarding it over HTTP to an ESP32 device operating in Access Point mode. Concurrently, the ESP32 retrieves real-time inertial data, namely, acceleration and angular velocity—using the MPU6050 sensor via the I2C communication protocol. The ESP32 then merges the encoder and inertial data into a unified JSON object, which is made accessible through a web interface for real-time monitoring and visualization.

The step-by-step procedure of the data collection can be summarized as follows:

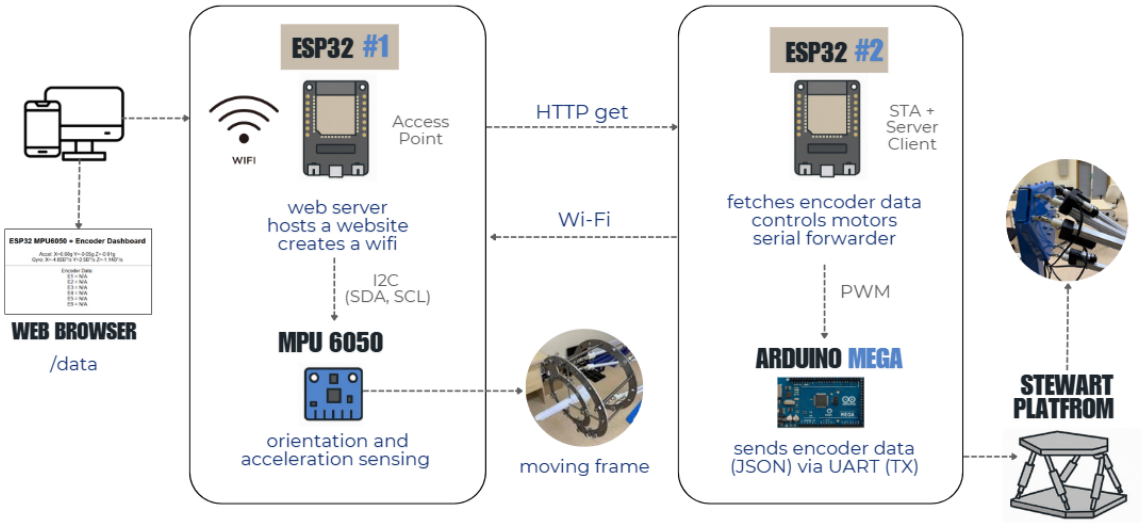

Figure 3-11: Wi-Fi-connected telemetry and motor control for the data collection procedure

1. Encoder data acquisition on Arduino Mega.
2. Data packaging and transmission to ESP8266.
3. Reception and validation on ESP8266
4. WiFi communication from ESP8266 to ESP32
5. Inertial data collection on ESP32
6. Data integration and web serving

The diagram on Figure 3-12 presents the full actuator control chain. Each actuator is equipped with an incremental encoder to provide real-time position feedback based on shaft rotation, enabling closed-loop control.

These actuators are powered and controlled via DBH-12V motor drivers, which receive PWM signals and direction inputs from an Arduino Mega 2560 microcontroller. The Arduino Mega handles both motor control and encoder reading, acting as the central node for motion execution and local feedback collection. To interface with a secondary processing unit, an ESP32-12E module is used. The ESP32 handles

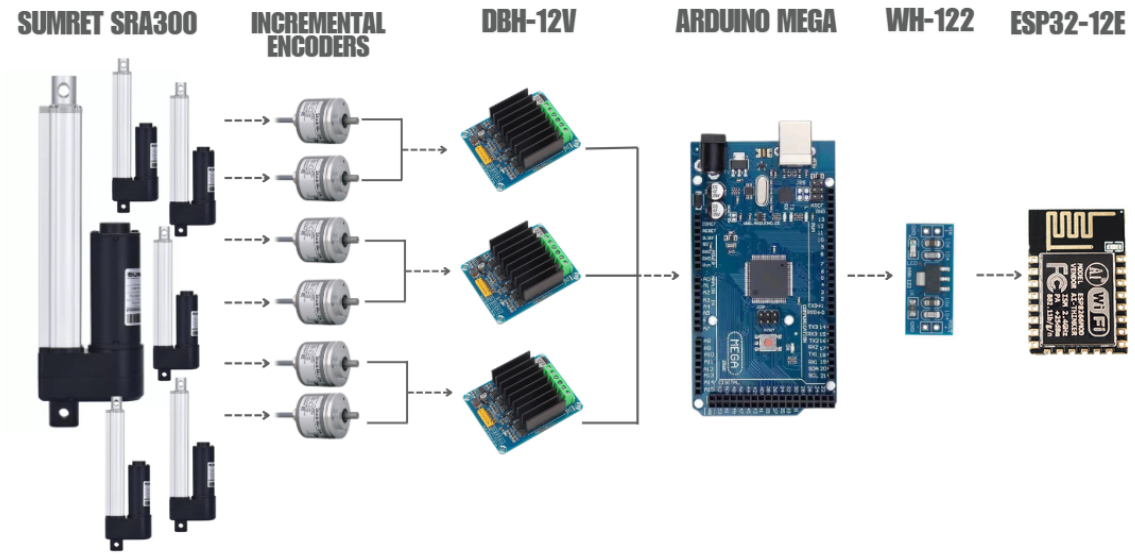

Figure 3-12: Hardware components

wireless communication and additional sensor integration. Since the Arduino Mega operates at 5V logic and the ESP32 at 3.3V logic, a WH-122 level shifter is placed between them to ensure safe and reliable UART communication. A MPU6050 inertial measurement unit (IMU) is attached to the moving platform. It provides 3-axis accelerometer and gyroscope data for pose estimation. it is connected to another ESPm device serving as a web server host.

This setup enables the Arduino Mega to transmit synchronized actuator length data to the ESP32, which can then combine it with IMU readings (e.g., from an MPU6050 mounted on the platform) for real-time pose estimation. The collected data serves as input to a machine learning model designed to correct forward kinematics errors, enhancing the system's accuracy for precision applications such as robotic bone fracture alignment.

Figure **??** presents the wiring schematic used to interface the microcontroller with multiple peripheral modules. In this configuration, the microcontroller communicates with a series of input/output devices through both analog and digital pins. The teal-colored modules represent intermediary control units (e.g., motor drivers, sensor breakouts), while the beige blocks correspond to actuators or sensor units. Each mod-

ule is connected via dedicated signal lines to designated pins on the microcontroller to ensure accurate and synchronized control and data acquisition. This hardware architecture forms the basis for real-time signal processing and feedback control in the developed system.

To build a robust model, the robot's motion was exercised through a wide range of poses and trajectories. This included both moderate movements and poses near the edge of the workspace (where kinematic nonlinearity is highest). The platform was commanded to move in each degree of freedom (surge, sway, heave, pitch, roll, yaw) individually and in combination within the safe limits. By covering many configurations – including some near singular positions or extreme angles – the dataset was ensured to contain the platform's typical operating range as well as challenging cases [39]. In each experiment trial, six actuator lengths from the encoders were recorded and the IMU's orientation continuously as the platform moved. After multiple sessions, a large dataset (on the order of several thousand timestamped samples) of synchronized encoder and IMU readings was created. These data would later be used to train and validate the pose error correction model.

Chapter 4

Results and Discussion

4.1 Ground Truth Definition

In the system, the ground truth orientation of the moving platform is provided by the IMU's measurements (after appropriate filtering), since the IMU directly senses the platform's actual orientation in space. The IMU used contains a 3-axis gyroscope, accelerometer, and magnetometer, enabling it to compute orientation reliably by fusing these sensors' data [40]. The data was run through a sensor fusion filter - Kalman Filter - to obtain a stable orientation estimate with reduced noise [41]. The filter combines high-rate gyro readings (integrated to track orientation changes) with accelerometer and magnetometer data (to correct drift with respect to gravity and heading). This yields the platform's orientation as Euler angles in real time. This filtered IMU orientation is considered as "true" orientation of the platform's top plate. Before using the IMU output as ground truth, an initial calibration to align frames was performed. When the platform is in a known reference pose (e.g. level and centered), the IMU's orientation reading was tracked and served as the reference (zero-error) orientation. This accounts for any constant offset between the IMU's internal coordinate frame and the platform's coordinate frame. After this calibration step, the IMU can provide orientation in the platform's reference frame directly. Thus, at any time t, the ground-truth orientation $O_{\text{true}}(t)$ is given by the IMU (filtered) output. For the position, obtaining a ground-truth is more challenging (since an IMU alone cannot

give absolute position without drift). In the case of the proposed system, there's a reliance on forward kinematics for position and focus on correcting orientation error, because orientation alignment is especially critical for fracture reduction and the IMU provides a trustworthy ground truth for it. Therefore, the pose error that this research aims to learn will primarily be an orientation error. The forward kinematics (FK) of the Stewart platform, using the encoders, gives an estimated pose $(P_{\text{est}}, O_{\text{est}})$ (position and orientation). The IMU gives the true orientation O_{true}. The orientation error was defined as $\Delta O = O_{\text{true}} - O_{\text{est}}$ (in terms of rotation angles). In practice, we represent O_{est} and O_{true} as Euler angles (yaw, pitch, roll), and compute the difference in each angle. We ensure to unwrap these angles to avoid discontinuities (e.g., distinguishing a $+350^\circ$ from a -10° reading). The result is a 3-dimensional error vector (for roll, pitch, yaw) for each timestamp. This orientation error, along with any detectable position error (if we had ground truth for position), constitutes the target output for our learning model. By formulating the error this way, we are following a model-error compensation approach: rather than predicting pose from scratch, the model will learn the residual errors of the FK model as a function of the robot's configuration [39].

With the data and ground truth established, it is now needed to formalize the machine learning problem. Each data sample corresponds to a robot configuration at time t. We take the actuator encoder lengths as the input features to the model. There are six actuators, so the input can be represented as a 6-dimensional vector:

$$\mathbf{x}(t) = [L_1(t), L_2(t), \ldots, L_6(t)]^T \tag{4.1}$$

where $L_i(t)$ is the length of actuator i at time t. These lengths (or equivalently, their extension from a home position) uniquely define the platform's pose in an ideal model. However, due to real-world imperfections, the forward kinematics using these lengths may not perfectly match the actual pose. The output of the learning model is defined as the pose error: specifically, the difference between the pose predicted by ideal forward kinematics and the actual pose as given by the sensors. As discussed,

this is primarily the orientation error. We denote the error as:

$$\mathbf{y}(t) = [\Delta\text{roll}(t), \Delta\text{pitch}(t), \Delta\text{yaw}(t)]^T \tag{4.2}$$

which is the orientation error vector (in degrees or radians). Each component, like Δroll, is computed as $\text{roll}_{\text{IMU}} - \text{roll}_{\text{FK}}$ at that time. Thus, the learning task for the model is as follows: Given the six actuator lengths, predict the orientation error of the Stewart platform. In other words, the model learns the mapping

$$f : \mathbf{x} \to \mathbf{y} \tag{4.3}$$

that best fits our observed data. The input-output formulation was chosen to leverage the existing kinematic model and only learn the residual errors. This approach combines model-based and data-driven methods: the nominal kinematic model provides an initial pose estimate, and a learned function handles the hard-to-model errors. By using the actuator lengths as inputs, we treat the relationship between pose error and platform configuration as a "black box" function to be learned. Prior research in parallel robot calibration has shown that using joint positions as inputs and measured pose errors as outputs in a regression model (e.g., an ANN or SVM) is effective for capturing complex error trends without explicitly modeling every error source.

4.2 Data Preprocessing

Before training the model, the collected raw data must be preprocessed to ensure quality and compatibility with the learning algorithm. We applied the following preprocessing steps:

- The first step was to make sure each input-output pair is correctly synchronized and aligned in time. Although data were recorded with timestamps, minor timing offsets can occur. We interpolated slower signals if necessary so that for every timestamp t we have a complete feature vector of six lengths and

the corresponding IMU orientation. In practice, because our system logged all sensor readings in one loop, the data were inherently synchronized. We trimmed any initial or ending portions where all sensors did not have readings (for example, if the IMU started slightly earlier than the encoders or vice versa). Each data sample is thus a tuple $(L_1, \ldots, L_6, \Delta\text{roll}, \Delta\text{pitch}, \Delta\text{yaw})$ all taken at the same time.

- Because raw IMU data can be noisy due to vibration of the platform and sensor noise, filtering and noise reduction techniques such as Kalman filter were applied to improve the signal quality. This filtering fuses noisy accelerometer and gyroscope data to estimate a smooth, accurate, and drift-corrected orientation or motion state in real time. The encoder readings are typically very precise, but if any high-frequency noise was present (e.g., due to electrical noise in readings), a light smoothing was applied there as well. The orientation data was as well ensured to have continuous angle representation – for instance, if yaw passed through 180° to -179°, it was unwrapped to avoid a sudden jump in the error computation.

- The dataset was scanned for any obvious outliers or faulty readings. For example, IMU may have experienced a momentary disturbance (probably due to the magnetic interference) that caused a sudden incorrect orientation reading, those samples are removed. Outliers were detected by looking at consecutive differences and thresholding extreme changes that are physically impossible. Removing these outliers prevents the model from being misled by erroneous data points.

- To aid the neural network training, the input and output values were normalized. The six actuator lengths, measured in millimeters, vary roughly within a certain range (for example, each leg might range 0–750 mm of extension). These inputs were normalized to a consistent scale (zero-mean and unit-variance normalization). This means we subtract the mean length and divide by the standard deviation (computed over the training set) for each actuator's data. Af-

ter normalization, all input features are dimensionless with roughly unit scale, which helps the neural network converge faster and prevents any one feature (e.g., a length of 150 mm) from dominating due to scale. Since orientation errors might be on the order of a few degrees, we could either leave them as-is (small values near zero) or scale them up for numerical stability. In our case, we converted angles to radians and kept them unscaled (as they were already small), but one could scale them by a constant factor if needed. The key is that both inputs and outputs are within reasonable ranges for the network (typically on the order of $[-1, 1]$ or so after scaling).

- Before training, the processed dataset was parted into subsets for training, validation, and testing. The dataset was shuffeled (or the list of motion trials) to ensure random distribution of samples, then split approximately 70% of the data for training, 15% for validation, and 15% for testing. The training set is used to fit the model weights, the validation set is used to tune hyperparameters and decide when to stop training (early stopping), and the test set is held out to evaluate the final model's performance. The data from a given continuous motion trial was checked to not to be split across train and test arbitrarily (to avoid highly correlated consecutive points leaking into the test set). Instead, it was grouped by trajectories: some entire motion sequences were designated for testing to evaluate generalization to new motions.

These preprocessing steps lead to the clean dataset of input vectors (encoder lengths) and target output vectors (pose errors). This processed dataset is then used to train the regression model.

4.3 Model Architecture

The model follows the architecture of a fully connected deep neural network (DNN) for regression. The neural network model designed for predicting pose error from actuator lengths is a deep feedforward architecture composed of three fully connected

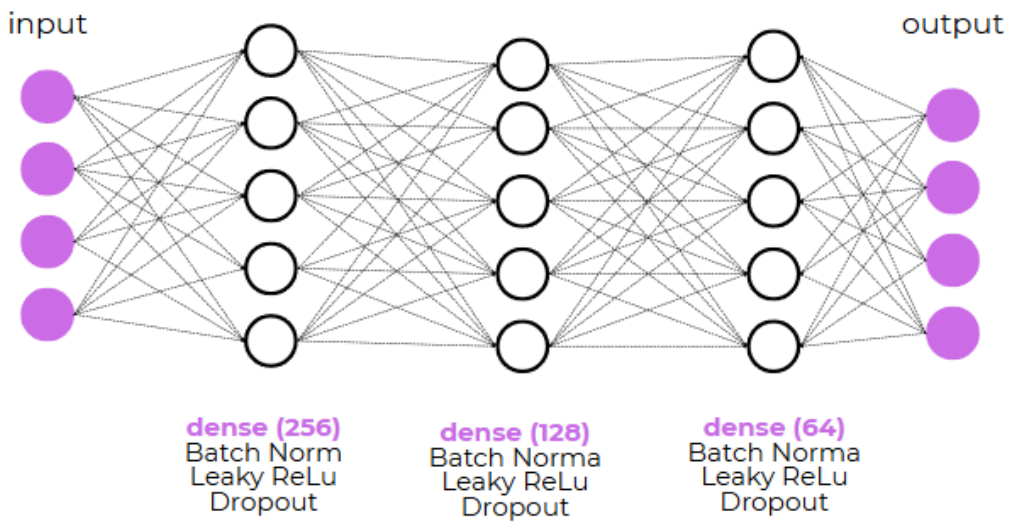

Figure 4-1: Architecture of the regression neural network used for pose error compensation in the Stewart platform

layers with 256, 128, and 64 neurons respectively. Each layer is followed by Batch Normalization, Leaky ReLU activation, and Dropout for improved training stability and regularization. The model accepts a 6-dimensional input vector (representing actuator lengths) and produces a 6-dimensional output corresponding to the predicted translation and rotation correction values. The architecture is illustrated in Figure 4-1.

This architecture was chosen to progressively learn high-level features from the actuator data through the large first hidden layer and then compress these features in later layers. The use of Batch Normalization (BN) after each dense layer helps stabilize and accelerate training by normalizing the layer inputs to a consistent scale. This allows the network to train faster and achieve higher learning rates without diverging [42]. A LeakyReLU activation is utilized instead of standard ReLU to avoid dead neurons. The leaky slope of 0.1 ensures a small gradient is sustained for negative inputs. Additionally, Dropout regularization (20% dropout) is applied after each activation. Dropout randomly deactivates a fraction of neurons during training, which

helps prevent overfitting by forcing the network to learn redundant representations. Together, these design choices (BN + LeakyReLU + Dropout) improve the network's generalization and training stability. The final output layer is linear, producing real-valued pose error predictions in an unconstrained range (since pose errors can be positive or negative). This linear output is appropriate for a regression task where we want the network to directly predict the error values without any predefined bounding or transformation.

4.4 Evaluation

The neural network was trained using a Mean Squared Error (MSE) loss function, which is appropriate for this multi-output regression problem. MSE computes the average of the squared differences between predicted and true error values, penalizing larger errors more strongly and yielding a smooth, convex loss landscape for optimization. In addition to MSE as the optimization objective, the Mean Absolute Error (MAE) metric was tarcked on both training and validation sets. MAE (the average of absolute differences) provides an interpretable measure of average error in the same units as the output, complementing MSE by being less sensitive to outliers. The main reason for choosing the MSE loss metrics over other types lies in its simplicity, predictability, and strong sensitivity to large errors, which makes it effective for penalizing significant deviations during model training.. Monitoring both MSE and MAE gives a fuller picture of performance during training. For optimization, the Adam optimizer (Adaptive Moment Estimation) was employed with its default learning rate of 0.001. Adam is a stochastic gradient descent algorithm that adapts the learning rate for each parameter, combining the advantages of momentum and RMSprop. It is known to be computationally efficient and well-suited for problems with large data and parameters, and it generally converges faster with less tuning of the learning rate. Adam's adaptive learning rate behavior was beneficial given the different scales and units in our problem (even after normalization), as it automatically adjusted the step sizes for each weight during training. Training was performed

in mini-batches of 32 samples (batch size = 32), which is a typical setting that offers a good balance between gradient estimate stability and training speed. The total number of epochs is below 50 because the visible improvements in validation loss were not observed. In practice, an early stopping criterion was implemented to prevent overfitting: the training was stopped when the validation loss ceased to improve for a certain number of epochs (patience window). In this case, the model stopped at 41 epochs because no further improvement in validation MSE was observed beyond that point. A learning rate scheduler (ReduceLROnPlateau) that automatically reduced the learning rate by a factor (e.g. 0.2) was also employed when the validation loss plateaued for 10 epochs, to fine-tune the later stages of learning. These measures ensured that the model did not over-train on the training data and that it achieved the best possible validation performance. During training, the MSE and MAE on both training and validation sets were recorded at each epoch to assess convergence. The network's error dropped rapidly in the first few epochs, indicating that it was quickly learning the actuator-to-pose-error mapping. For example, the training MSE started near 1.0 (in normalized units) at the first epoch and fell by an order of magnitude within the first 5–10 epochs. The validation MSE showed a similar downward trend, decreasing from an initial 0.065 to around 0.0063 by epoch 41. Meanwhile, the MAE metrics also declined significantly (training MAE from about 0.75 to 0.21, and validation MAE from about 0.20 to 0.063, all in normalized error units). By epoch 40–41, the curves for both training and validation loss had flattened, indicating convergence. Notably, the final validation error was extremely low and even slightly below the training error. This suggests that the model generalized well to the validation data, likely aided by the regularization techniques (dropout and batch normalization) used during training. The small gap between training and validation errors in the final epochs, with no divergence, indicates that overfitting was successfully mitigated. The training graphs demonstrate smooth and stable learning – the validation loss decreases steadily without large spikes, and no significant gap opened between training and validation errors over time, which would be a warning sign of overfitting (see Figure 4-2).

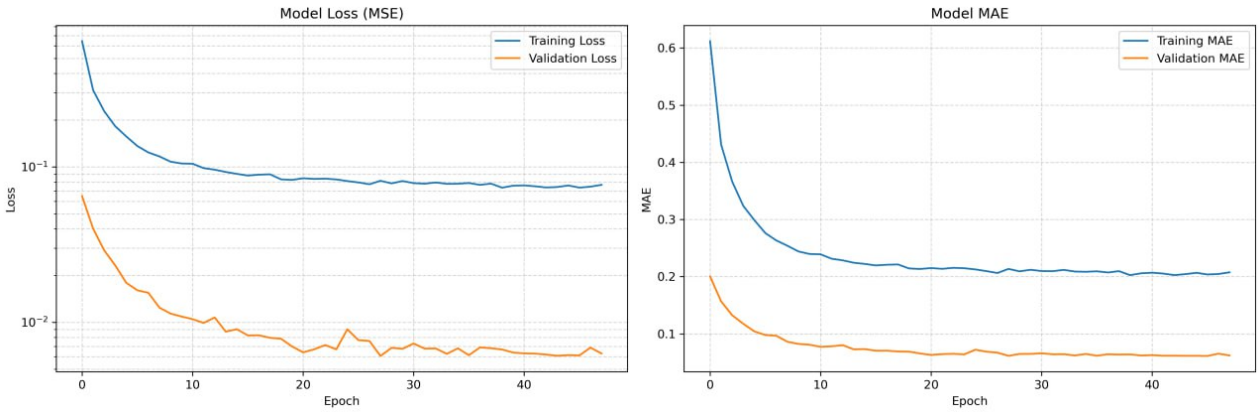

Figure 4-2: Model error metrics. (Left) Mean Squared Error (MSE) for training and validation. (Right) Mean Absolute Error (MAE) for training and validation.

In summary, the pose-error prediction model is a deep feedforward neural network with three hidden layers (256–128–64 neurons) and extensive use of batch normalization and dropout for robust learning. The model was trained using MSE loss and the Adam optimizer, with carefully tuned hyperparameters (batch size, learning rate schedule, early stopping) to ensure reliable convergence. Thanks to these choices, the network can accurately predict the 6-DoF pose error of the Stewart platform from the actuator lengths, as evidenced by the low validation errors and the converged training process. This model will serve as a core component in our Stewart platform calibration methodology, enabling real-time compensation of pose errors based on the learned mapping from actuator data to pose error.

4.5 Integration Strategy for Real-Time Operation

Ultimately, the trained model needs to be integrated into the Stewart platform's real-time control system to correct pose estimation online. The goal is to have the robot utilize the improved pose estimation in its feedback loop or navigation system during operation. The integration will follow the definite step-by-step procedure:

- Sensor Data Acquisition: During real-time operation, at each control cycle, the system reads all six actuator encoder values. These represent the current configuration of the Stewart platform. Simultaneously, the IMU is still running

for safety, but in normal operation, we will not use the IMU in feedback (to avoid dependency on it during surgery). Instead, the IMU is primarily used for ground truth during development. The real-time controller thus relies on encoders (which are always available) for feedback.

- Baseline Pose Computation: The control software computes the platform's pose using the known forward kinematics function $FK(L_1, \ldots, L_6)$. This yields an estimated pose (position and orientation) of the bone or platform. This is the same calculation the system would normally use in absence of the ML model, and it's very fast (a few milliseconds or less, often using Newton-Raphson or closed-form solutions). Error Prediction: The same encoder readings $(L_1, \ldots, L_6)$ are fed into the trained neural network model (which has been deployed on the control PC or microcontroller). The network performs a forward pass computation to output $\Delta\text{roll}, \Delta\text{pitch}, \Delta\text{yaw}$ – the predicted orientation error for the current configuration.

- Pose Correction: The predicted error is then added to the baseline FK pose to get the corrected pose estimate. For example, the system maintains an estimate of the platform's orientation. If the FK gave an orientation of (roll=5.0°, pitch=2.0°, yaw=10.0°) and the network predicts an error of Δroll = -0.5°, Δpitch = 1.0°, Δyaw = -0.2°, then we update the pose estimate to (roll=4.5°, pitch=3.0°, yaw=9.8°). This corrected pose is our best estimate of the actual platform orientation.

Over time or after any hardware changes, the error characteristics might change. The examples may include the wear of joints and other hardware parts or the re-calibration of encoders. That's why the integration strategy must account for the possibility of re-running the data collection and retraining procedure to update the model. This might be integrated into the routine maintenance of the system through the automation of the training procedure, ensuring long-term accuracy and adaptability to new configurations of the system. In essence, the model can learn new error patterns if the Stewart platform's behavior changes.

These steps are required so that the Stewart platform's controller continuously self-corrects its pose estimation during operation. This allows the system to achieve much higher accuracy in positioning the femur for fracture reduction than would be possible with the theoretical model alone. Importantly, this correction is achieved using only the encoders and a one-time trained neural network – the IMU is not required during the actual surgery, which simplifies the system and removes potential drift issues in long procedures. Moreover, the exclusion of the IMUs from the end purpose eliminates the cumulative error posed by IMU, thereby contributing to the self-containment of the system. The integrated solution takes advantage of the data-driven model's accuracy and the robustness of having it embedded in real time. The the model-based and learned approaches were effectively combined so that the model-based FK provides a quick initial guess, and the learned NN provides a refinement, yielding an accurate pose estimate on the fly. This approach has proven to significantly enhance the Stewart platform's pose accuracy and robustness, which is crucial for the precise demands of orthopaedic fracture reduction.

Chapter 5

Conclusion

5.1 Conclusion

This thesis presented the development of a novel robotic system for long bone fracture reduction, with a specific focus on femoral realignment. The proposed system is centered around a Stewart platform and integrates mechanical design, sensor instrumentation, and machine learning-based pose correction. The approach aims to enhance both the accuracy and safety of the fracture reduction process compared to traditional manual methods and existing robotic solutions.

The use of a robotic system offers clear advantages over manual fracture reduction techniques that rely heavily on the surgeon's experience and physical effort, often leading to variability in outcomes, extended procedure times, and increased risk of repeated fracture in the near future. In contrast, the robot provides consistent and precise control in six degrees of freedom, enabling reproducible, data-driven realignment of fractured segments while minimizing soft tissue damage. This consistency can significantly reduce surgeon fatigue, improve surgical outcomes, and enhance patient recovery.

Compared to other robotic systems for fracture reduction, the proposed Stewart platform-based design stands out for its e integration of a machine learning model for real-time pose error correction marks a significant innovation in the system. Traditional inverse kinematics models fail to account for real-world deviations caused

by mechanical non-linearities, system noise, or biological variability such as soft tissue resistance. By training a neural network to estimate pose error directly from actuator lengths, the system gains the ability to self-correct and adapt dynamically. This eliminates the need for external sensors like IMUs during surgery, streamlines the control system, and increases robustness against drift and cumulative errors. The ML-enhanced framework represents a step toward intelligent, self-compensating robotic systems in orthopedic surgery.

In summary, this work demonstrates that combining a parallel mechanism with data-driven correction mechanisms can significantly enhance the precision and reliability of femur fracture reduction. The system not only bridges the gap between clinical requirements and robotic capabilities but also paves the way for future autonomous surgical platforms where machine learning plays a central role in error correction and adaptive control.

5.2 Future directions

For further improvements in the alignment precision and accuracy several objectives can be explored. First of all, the primary focus should be on an enhancement of the noise cancellation model. The improvements may include the introduction of the reinforcement learning model for movement optimization. The introduction of Physics-Informed Neural Networks (PINNs) can further enhance the system's precision by incorporating physical constraints into the learning process, enabling the model to generalize beyond data alone. In addition, a sophisticated control system for the visual monitoring of the distal segment orientation from the fluoroscopy can be added. High-precision force and torque sensors would allow better control over applied forces, while optical tracking or ultrasound-based navigation can improve localization accuracy and reduce the need for surgeon intervention.

To further refine and streamline the process, the ML-based 3D reconstruction can be implemented with the help of masked auto-encoders and visual encoders. This would eliminate the need for the manual reconstruction which sometimes may not be

accurate in the presence of artifacts or implants. A fully functional website featuring real-time sensor telemetry and X-ray data visualization would significantly enhance the usability and overall value of the final system.

Another critical step in the advancement of this robotic system is the development of robust and safe path-planning algorithms, such as Rapidly-Exploring Random Trees (RRT) or other optimized trajectory generation methods tailored for anatomical realignment. While the current system is capable of precise end-point alignment through inverse kinematics and machine learning-based correction, it lacks a mechanism for generating continuous, safe, and anatomically informed paths between the initial and target poses. It is of extreme importance as not only bones and soft tissues are in danger during the operation, but also the nerves, major blood vessels surrounding the fracture. Damaging them may lead to sever complications, including nerve damage and pulmonary hemorrhage. Therefore, path planning must not only be geometrically valid but also clinically safe, considering anatomical constraints and varying patient-specific conditions. This challenge will be resolved in collaboration with the orthopedic surgeons, radiologists, and trauma specialists for determining acceptable manipulation forces and validating simulated reduction trajectories for biologically aware path-planning frameworks.

Integrating such planning algorithms with real-time feedback and safety constraints will mark a substantial step toward semi-autonomous and fully autonomous robotic fracture reduction systems suitable for clinical deployment. To bring these advancements to the clinical practices, the focus on these objectives may expand the concept into an innovative orthopedic device.

Bibliography

[1] Ju Zhang, Duane Malcolm, Jacqui Hislop-Jambrich, C. Thomas, and Poul Nielsen. An anatomical region-based statistical shape model of the human femur. *Computer Methods in Biomechanics and Biomedical Engineering: Imaging Visualization*, 2, 02 2014.

[2] Radiopaedia Contributors. Tibial fracture (transverse diaphyseal), 2025. Accessed: March 20, 2025.

[3] AO Foundation. Pediatric femoral shaft fracture (32-d/5.1) definition, 2025. Accessed: March 20, 2025.

[4] Radiopaedia Contributors. Spiral fracture, 2025. Accessed: March 20, 2025.

[5] OrthoBullets Contributors. Femoral shaft fractures, 2025. Accessed: March 20, 2025.

[6] Radiopaedia Contributors. Segmental fracture, 2025. Accessed: March 20, 2025.

[7] Chor-Wing Sing, Tzu-Chieh Lin, Sharon Bartholomew, J Simon Bell, Corina Bennett, Kebede Beyene, Pauline Bosco-Lévy, Amy Hai Yan Chan, Manju Chandran, Ching-Lung Cheung, Caroline Y Doyon, Cécile Droz-Perroteau, Ganga Ganesan, Sirpa Hartikainen, Jenni Ilomaki, Han Eol Jeong, Douglas P Kiel, Kiyoshi Kubota, Edward Chia-Cheng Lai, Jeff Lange, E Michael Lewiecki, Jiannong Liu, Kenneth K C Man, Mirhelen Mendes de Abreu, Nicolas Moore, James O'Kelly, Nobuhiro Ooba, Alma B Pedersen, Daniel Prieto-Alhambra, Ju-Young Shin, Henrik T Sørensen, Kelvin Bryan Tan, Anna-Maija Tolppanen, Katia M C Verhamme, Grace Hsin-Min Wang, Sawaeng Watcharathanakij, Hongxin Zhao, and Ian C K Wong. Global epidemiology of hip fractures: a study protocol using a common analytical platform among multiple countries. *BMJ Open*, 11(7), 2021.

[8] Yu Liu, Hao Zhang, Xinxin Chen, Yiming Wang, et al. Incidence and influence factors of venous thromboembolism in hospitalized patients with traumatic rib fractures: A retrospective cohort study. *International Journal of Surgery*, 118:106199, 2024.

[9] Samuel M. Galvagno, Charles E. Smith, and Thomas M. Scalea. Risk factors for pneumonia following rib fractures: A systematic review and meta-analysis. *The American Journal of Emergency Medicine*, 38(5):967–973, 2019.

[10] Federico M. Pieracci, Kaitlyn Leasia, Zachary Bauman, and Emilie A. Eriksson. Chest trauma: Current recommendations for rib fractures. *Trauma Surgery Acute Care Open*, 5(1):e000469, 2020.

[11] C. Cooper, G. Campion, and L. J. Melton III. Hip fractures in the elderly: A worldwide projection. *Osteoporosis International*, 7(5):407–413, 1997.

[12] Eva Y. Cheung, Alisha Y. Wang, Carmen W. Ling, Kwok-Leung Cheung, Wing-Hoi Cheung, and Kenneth M. C. Cheung. Worldwide hip fracture projections: Despite declining rates, the absolute number of hip fractures will nearly double by 2050. *Journal of Bone and Mineral Research*, 38(7):1330–1340, 2023.

[13] Noa H. M. Ponds, Jochem H. Raats, Devon T. Brameier, Henk Jan Schuijt, Lisa Cooper, Abigail Sagona, Houman Javedan, and Michael J. Weaver. Beyond mortality: Severely frail femur fracture patients can regain independence after surgery. *Journal of Clinical Medicine*, 13(11):3197, 2024.

[14] Olof Johnell, John A. Kanis, Anders Odén, Hans Johansson, and Eugene McCloskey. Risk of subsequent fracture after prior fracture among older women. *Osteoporosis International*, 29(3):709–717, 2018.

[15] Brenna M. Tang, Denise Esserman, Helen Mogun, Jerry Avorn, M. Alan Brookhart, and Sebastian Schneeweiss. Osteoporosis treatment after osteoporotic fractures: Data from a large us health care delivery system. *Endocrine Practice*, 28(6):621–629, 2022.

[16] Olof Johnell and John A. Kanis. Epidemiology of hip fracture: Worldwide geographic variation. *Osteoporosis International*, 17(12):1726–1733, 2006.

[17] Danupong Buttongkum, Pairat Tangpornprasert, Chanyaphan Virulsri, Numphung Numkarunarunrote, Chavarin Amarase, Thananop Kobchaisawat, and Thanarat Chalidabhongse. 3d reconstruction of proximal femoral fracture from biplanar radiographs with fractural representative learning. *Scientific Reports*, 13:455, 2023.

[18] American Academy of Orthopaedic Surgeons (AAOS). Clinical practice guideline: Management of hip fractures in the elderly, 2022. Accessed: March 20, 2025.

[19] Christian Krettek. Percutaneous reduction techniques. In *AAOS 2016 Specialty Day, Orthopaedic Trauma Association (OTA)*, Hannover Medical School, Germany, 2016. Available from: Hannover Medical School.

[20] Michael L. Robinson and Benedict A. Rogers. The role of robotics in trauma and orthopaedics. *Orthopaedics and Trauma*, 37(4):239–245, 2023.

[21] Vaibhav Kumar, C Uday Chandran, and Kumar Anshuman. Application of robotics in orthopaedic surgery. *International Journal of Orthopaedics Sciences*, 6(4):602–606, 2020.

[22] Wei Kou, Peiqing Zhou, Jihong Lin, Shaolong Kuang, and Lining Sun. Technologies evolution in robot-assisted fracture reduction systems: a comprehensive review. *Frontiers in Robotics and AI*, 10, 2023.

[23] H.A. Paul, W.L. Bargar, B. Mittelstadt, and B.L. Musits. Development of a surgical robot for cementless total hip arthroplasty. *Clinical Orthopaedics and Related Research*, 285:57–66, 1992.

[24] Martin Roche. The mako robotic-arm knee arthroplasty system. *Archives of Orthopaedic and Trauma Surgery*, 141:2043–2047, 2021.

[25] Simon M. Bolam, Sébastien Lustig, Elvire Servien, Martin Seidel, and Cédric Batailler. Introduction of rosa robotic-arm system for total knee arthroplasty is associated with a minimal learning curve for operative time. *Journal of Experimental Orthopaedics*, 9:84, 2022.

[26] Simon M. Bolam, Sébastien Lustig, Elvire Servien, Martin Seidel, and Cédric Batailler. Unsatisfactory accuracy of recent robotic assisting system rosa for total knee arthroplasty. *Journal of Experimental Orthopaedics*, 9:85, 2022.

[27] Wei Kou, Peiqing Zhou, Jihong Lin, Shaolong Kuang, and Lining Sun. Technologies evolution in robot-assisted fracture reduction systems: a comprehensive review. *Frontiers in Robotics and AI*, 10, 2023.

[28] Ravi Khakha, Panagiotis Gikas, Panagiotis Paschos, and Daniel Kendoff. Robotic assisted total knee arthroplasty: a clinical and technical review. *EFORT Open Reviews*, 8(1):1–13, 2023.

[29] S. Walgrave and S. Oussedik. Comparative assessment of current robotic-assisted systems in primary total knee arthroplasty. *Bone & Joint Open*, 4(1):13–18, 2022.

[30] Author(s) Name(s).

[31] A. Majidifakhr, M. Javad, M. T. Ahmadian, and B. Tarvirdizadeh. Study on a robotic-assisted femoral shaft fracture reduction system using a stewart platform. *Journal of Medical Robotics Research*, XX.

[32] Paul D. Korytkowski, John M. Panzone, Osama Aldahamsheh, Mohammed Mubarak Alkhayarin, Hanaa Omar Almohamad, and Abduljabbar Alhammoud. Open and closed reduction methods for intramedullary nailing of femoral shaft fractures: A systematic review and meta-analysis of comparative studies. *Journal of Clinical Orthopaedics and Trauma*, 44:102256, 2023.

[33] Jing-Xin Zhao, Changsheng Li, Hongliang Ren, Ming Hao, Li-Cheng Zhang, and Pei-Fu Tang. Evolution and current applications of robot-assisted fracture reduction: A comprehensive review. *Annals of Biomedical Engineering*, 2019.

[34] Wei Kou, Peiqing Zhou, Jihong Lin, Shaolong Kuang, and Lining Sun. Technologies evolution in robot-assisted fracture reduction systems: a comprehensive review. *Frontiers in Robotics and AI*, Volume 10 - 2023, 2023.

[35] Xianzheng Zhou, Yimiao Chen, Genyuan Miao, Yanchao Guo, Qinhe Zhang, and Jianping Bi. Computer-aided robotics for applications in fracture reduction surgery: Advances, challenges, and opportunities. *iScience*, 28(1):111509, 2025.

[36] Maximilian Faschingbauer, Hinrich Heuer, Klaus Seide, Robert Wendlandt, Matthias Münch, Christian Jürgens, and R. Kirchner. Accuracy of a hexapod parallel robot kinematics based external fixator. *The International Journal of Medical Robotics and Computer Assisted Surgery*, 11, 10 2014.

[37] Wei Kou, Peiqing Zhou, Jihong Lin, Shaolong Kuang, and Lining Sun. Technologies evolution in robot-assisted fracture reduction systems: a comprehensive review. *Frontiers in Robotics and AI*, 10, 11 2023.

[38] Minghe Liu, Jian Li, Hao Sun, Xin Guo, Bokai Xuan, Lifang Ma, Yuexuan Xu, Tianyi Ma, Qingsong Ding, and Baichuan An. Study on the modeling and compensation method of pose error analysis for the fracture reduction robot. *Micromachines*, 13(8), 2022.

[39] Yongbin Song, Wenjie Tian, Yanling Tian, and Xianping Liu. Calibration of a stewart platform by designing a robust joint compensator with artificial neural networks. *Precision Engineering*, 77:375–384, 2022.

[40] Rodrigo Medeiros, Guilherme Pimentel, and Rafael Garibotti. An embedded quaternion-based extended kalman filter pose estimation for six degrees of freedom systems. *Journal of Intelligent Robotic Systems*, 102, 05 2021.

[41] Xiafei Chen, Hai Zeng, Zening Chen, Xue Jiang, Lijie Zhang, and Xiaoping Liu. An algorithm for stewart platform motion state estimation combining ukf, newton's method, and neural networks, 2025. Accessed: 2025-04-15.

[42] Sergey Ioffe and Christian Szegedy. Batch normalization: Accelerating deep network training by reducing internal covariate shift. 02 2015.